Thermobaric Effects on Double-Diffusive Staircases

Erica Rosenblum

August 16, 2015

1 Introduction

Under the sea ice of the polar oceans, warm salty water flows below the cold, fresh surface waters. Meanwhile, deep below the surface, geothermal heating warms the cold, salty waters of the deep Arctic. In each of these systems, an unstable temperature gradient competes with a stabilizing salinity gradient, creating conditions susceptible to two instabilities. One of these instabilities, called double-diffusive convection, is due to the fact that heat diffuses 100 times faster than salt. This instability can lead to the formation of thermohaline staircases in which a series of well-mixed, convective layers are separated by sharp interfaces in both temperature and salinity. A second instability that exists in this system, called the thermobaric instability, arises because cold water is more compressible than warm water and therefore becomes denser with pressure

In the Arctic, waters from the North Atlantic provide the warm, salty water in the aforementioned system, leading to the formation of double-diffusive staircases (Figure 1). Contained within this North Atlantic water is enough heat to melt all of the Arctic sea ice, were it transported to the surface [10],[13]. Processes controlling vertical heat flux in this area of the world are not well understood, but double-diffusive convection has been identified as an important mechanism [9], and may therefore play an important role in the rapid disappearance of the Arctic sea ice.

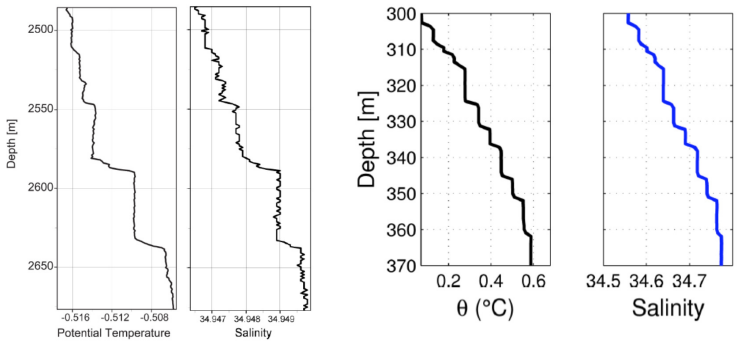

Figure 1: Examples of double-diffusive staircases found in the deep Arctic (left) and the shallow Arctic (right). Profiles taken from [13], [12]

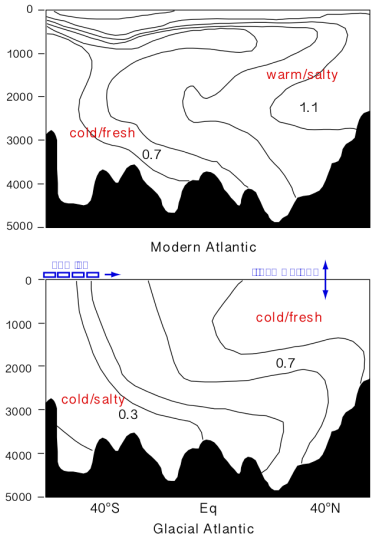

Figure 2: Cartoon description showing that the Atlantic was stably stratified by a salt gradient during the last glacial maximum, taken from [1]

Several thousand meters deeper, quietly sits the strongly salt-stratified waters of the deep Arctic. This water is slowly being heated from below by geothermal vents, again leading to a salt-stratified system that is heated from below. Double-diffusive staircases exist in this context as well, however, these staircases are notably thicker than than those found in the shallow Arctic (Figure 1).

This system is under a large amount of pressure and is potentially thermobarically unstable despite its strong salinity gradient. Interestingly, because this system has a strong salinity stratification and is being heated geothermally, it bears resemblance to the Atlantic Ocean during the last glacial maximum (Figure 2). It has been proposed that the bottom of this glacial Atlantic Ocean slowly warmed until an intense overturn occurred due to the thermobaric instability, leading to the rapid warming events observed in the paleoclimate record [1].

On the other side of the planet, cool, fresh surface water flows above warm, salty water near the coasts of Antarctica. Because the salinity is weakly stratified, it is susceptible to both double-diffusive convection and thermobaric instability, making it surprisingly similar to the deep Arctic, rather than its shallow Arctic counterpart. Susceptibility to these two instabilities has been observed in the Weddell sea. Here, the thermobaric instability has been invoked to explain periods of persistent deep convection and the formation of polynas [7], which have important implications for general ocean circulation as well as sea ice formation. Secondly, a recent study has suggested that double-diffusive convection may also have an important impact on the vertical heat transport in this area [11].

Despite their coexistence in these important and exciting areas of the ocean, neither the impact of thermobaricity on double-diffusive staircases, nor the influence of double-diffusion on the thermobaric instability has been examined. Here, we take the first step in studying how these two effects may interact by recreating a simple 1-D model of double-

diffusive staircases [4] and, for the first time, including thermobaric effects. Specifically, we examine how large changes in the thermal expansion coefficient affect the structure of the double-diffusive staircases found in the polar oceans. In the following section, these two instabilities are described in greater detail. In Section 3, we present the theory and numerical model which form the basis of our work, followed by our additions that allow us to include thermobaric effects in Section 4. Preliminary results are discussed in Section 5 and lastly, possible implications and future work is discussed in Section 6.

2 One system, two instabilities

When a pot of water is being heated from below, regular thermal convection can occur because cold water is denser than warm water. However, when a stable salinity gradient is added, the stability of the system depends on the ratio of the two background gradients. This quantity is well described by the density ratio: $R_0 = \frac{\beta \overline{S_z}}{\alpha \overline{T_z}}$, where $\overline{T_z}$ and $\overline{S_z}$ are the background temperature and salinity gradients, α is the thermal expansion coefficient, and β is the saline contraction coefficient. Thus, a larger density ratio describes a more stable system and vice versa (see Figure 3).

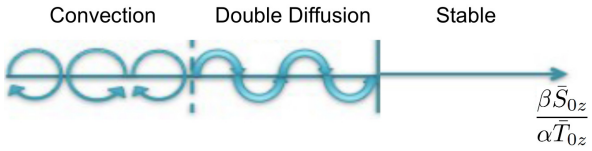

Figure 3: Cartoon describing the various stages of stability as function of the density ratio (see text) in a system with a negative temperature and salinity gradient.

2.1 Thermobaric instability

The thermal expansion coefficient is a negative value that is defined as

$$\alpha = \frac{1}{\rho_0}\left(\frac{\partial \rho}{\partial T} + \frac{\partial^2 \rho}{\partial T \partial P} + \frac{\partial^2 \rho}{\partial T^2} + ...\right), \tag{1}$$

where ρ_0 is a mean density, p is pressure, and T is temperature. The first term is negative and implies that the density of a parcel decreases as its temperature increases. The two nonlinear terms describe cabbeling and thermobaricity, respectively, which imply that α varies as both a function of pressure and temperature (Figure 4). This implies that by simply moving our system to a deeper pressure, the density ratio (and the stability) will decrease.

Moreover, as described by the thermobaric term, cold water is more compressible than warm water. Therefore, the thermal expansion coefficient increases with depth more rapidly for cold water. This allows for the possibility of a local instability in which a small perturbation to the system could cause a cool, fresh water parcel to fall towards the warmer, saltier part of the system. The colder parcel compresses enough (equivalently, α increases enough) to make the parcel denser than its salty surroundings causing it to continue to fall

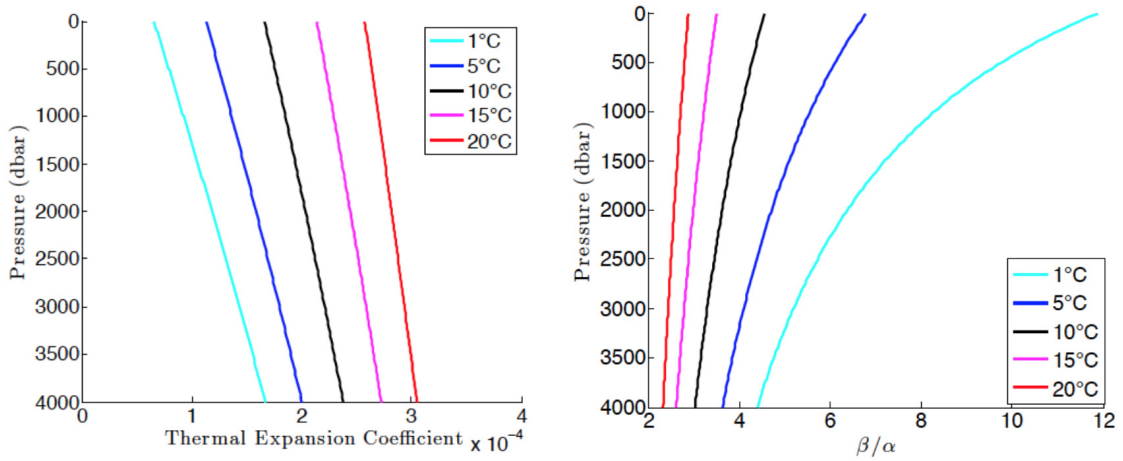

Figure 4: The thermal expansion coefficient (left) and the ratio of the salinity contraction coefficient to the thermal expansion coefficient (right) as a function pressure for several temperatures. The figures demonstrate that the thermal expansion coefficient increases with depth more rapidly in cold water compared to warm water.

towards the warm, salty part of the system [3],[6]). This instability is notably different and often stronger compared to regular thermal convection because it is internally driven by this thermobaric effect rather than continually forced at a boundary [2], [7].

2.2 Double-diffusive convection

Between the stable and fully convective states lives the double-diffusive instability (Figure 3). The initial instability of double-diffusive convection is well-described by a linear stability analysis [17]. Conceptually, it can be understood by imagining a small perturbation that causes a cool, fresh fluid parcel to fall toward the warm, saltier region of the system. The parcel will quickly diffuse in the surrounding heat but its salinity will remain nearly constant, causing the parcel to become warmer but remain fresher than its surroundings. Now much lighter than its environment, the parcel will float to a point somewhat higher than its initial position, where it will quickly diffuse its heat, maintaining its salinity to become denser than its surroundings and fall into the warm, salty area below. This fluid motion continues to oscillate, with the amplitude growing with each oscillation. Eventually, turbulent effects become dominant and a coherent structure emerges. This is called a thermohaline staircase, where each 'step' is made up of a cool, fresh layer over a warmer, saltier layer separated by a well-mixed interface.

3 Previous work

Turner and Stommel[14] performed the first laboratory experiments in which a stable salt gradient was heated from below. They found that within a few minutes, the bottom layer would overturn and form a well mixed layer. Within the hour, a series of well-mixed layers

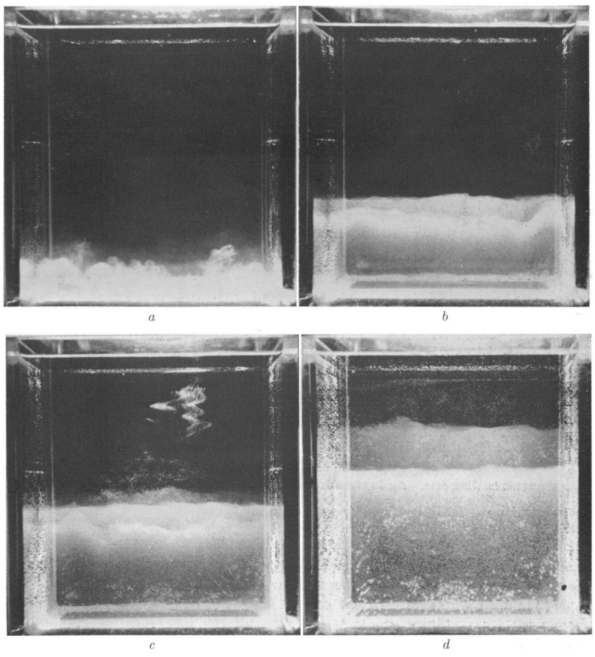

Figure 5: Image from Stommel and Turner 1964, showing results from a laboratory experiment where a stable salinity gradient is heated from below. (a) shows that one mixed layer has formed after 10 minutes. (b)-(d) shows that subsequent layers form after 25, 60 and 90 minutes, respectively.

(i.e. a double-diffusive staircase) formed in a similar fashion (Figure 5). In this section, we discuss a theory and numerical model that was developed to describe what had been seen in these laboratory experiments and form the foundation of our work.

3.1 Theory

Turner[15] describes the evolution of a system with an initially linear, negative salt gradient, $\overline{S_z}$, and a uniform background temperature, $\overline{T}$, that is heated from below by a constant heat flux, H (Figure 6). In particular, the evolution of the first layer as well as the growth and eventual formation of the second layer are discussed.

3.1.1 Evolution of the first layer

By implementing the conservation of heat and salt, the salinity (S_1), temperature (T_1) and thickness (h_1) of the first well mixed layer can be described by

$$\Delta S_1 = \frac{-1}{2} h \overline{S_z}, \qquad Ht = \rho c h_1 \Delta T_1, \tag{2}$$

where ΔS_1 and ΔT_1 are the change in salt and temperature across the top of the 1st layer (and are positive), t is time, ρ is the mean density of the system and c is the specific heat. To close this system of equations, we invoke

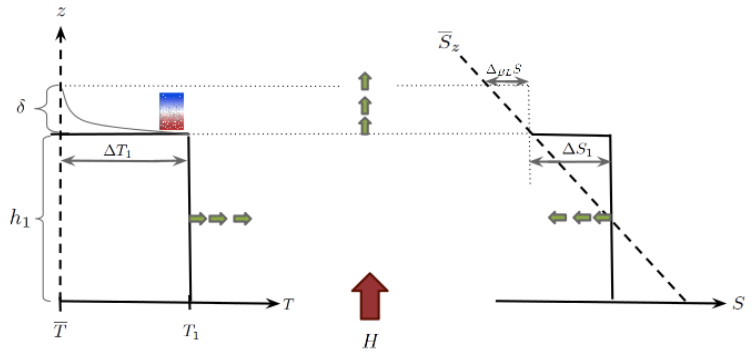

Figure 6: Cartoon depiction of the theory describing the formation of the first two mixed layers. The green arrows indicate that the layer warms, freshens and grows with time.

$$\alpha \Delta T_1 + \beta \Delta S_1 = 0, \tag{3}$$

which relates the two interfaces and implies that the density contributions from the heat and salt combine to create a continuous density profile (Figure 7).

By algebraically solving these equations, the expressions for the evolution of ΔT_1, ΔS_1 and h_1 are

$$h_1 = \sqrt{\left(\frac{\widetilde{H}_* t}{\widetilde{S}_*}\right)}, \qquad -\alpha g \Delta T_1 = \beta g \Delta S_1 = \sqrt{\widetilde{H}_* \widetilde{S}_* t}, \tag{4}$$

where $\widetilde{H}_*$ and $\widetilde{S}_*$ are the buoyancy fluxes, defined by

$$\widetilde{H}_* = \frac{-\alpha g H}{\rho c}, \qquad \widetilde{S}_* = \frac{-\beta g \overline{S_z}}{2}. \tag{5}$$

Thus, this layer, which is heated from below, warms and grows taller with time. As the layer grows, it overtakes the less salty water above and becomes fresher (Figure 6).

3.1.2 Evolution of boundary layer, formation of layer 2

While this layer grows, heat and salt are diffused through the top of the interface, causing a boundary layer to form. Because heat diffuses 100 times faster than salt, the diffusion of salt through the interface is neglected and a simple heat equation is used to describe its thermal evolution,

$$\frac{\partial \theta}{\partial t} = \kappa \frac{\partial^2 \theta}{\partial z^2}, \qquad \begin{aligned} \theta(z = h_1) &= T_1 \\ \theta(z \to \infty) &= \overline{T}, \end{aligned} \tag{6}$$

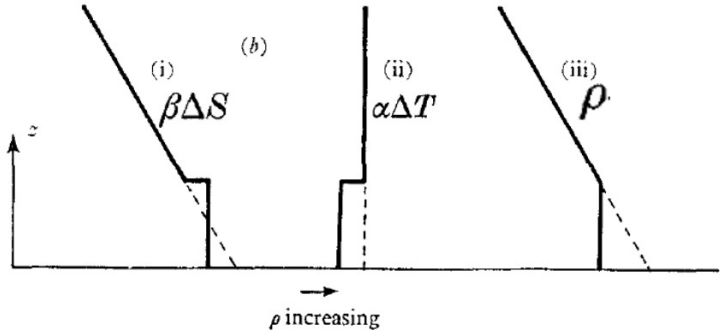

Figure 7: Cartoon depiction of equation (3)

where κ is the thermal diffusivity, θ is the temperature of the boundary layer and $\overline{T}$ is the initial uniform background temperature.

As heat diffuses through the boundary layer, cool, fresh water lies above increasingly warmer, salty water. These are the conditions necessary for the double-diffusive instability to occur. Turner suggests that this boundary layer will overturn and consequently form a second convective mixed layer when the temperature gradient grows strong enough such that it is linearly unstable to double-diffusive convection. The criterion for overturn is then given by Veronis[16], who found that the onset for double-diffusive convection between two freely moving boundaries is given by

$$R = R_T - \frac{\sigma}{\sigma + 1} R_S \geq \frac{27\pi^4}{4}, \tag{7}$$

where $R_T = \frac{-\alpha g \Delta_{BL} T \delta^3}{\kappa\nu}$, $R_S = \frac{\beta g \Delta_{BL} S \delta^3}{\kappa\nu}$, δ is the scaling length of the boundary layer, ν is the kinematic viscosity, and $\sigma = \frac{\nu}{\kappa}$ is the Prandtl number. Δ_{BL} is a positive value that signifies the change in temperature and salinity above the interface. Thus,

$$\Delta_{BL} T = T_1 - \overline{T}, \qquad \Delta_{BL} S = -\overline{S_z}\delta,$$

because we have assumed that the diffusion of salt through the top of the layer can be neglected (Figure 6).

3.2 Numerical model

Using the framework put forth in [15], Huppert[4] developed a one-dimensional numerical model that could describe this system with multiple (N) layers. However, some additional assumptions are included in this model:

- Loss of heat through the top of the staircase can be neglected in the heat budget.
- Only the top layer grows. Interior layers have a constant thickness unless they merge together to form a thicker layer.
- If two layers create a neutral density profile, the two layers merge.

- heat and salt fluxes across the interface are given by experimentally determined flux laws [5]:

$$\begin{aligned} \phi_i &= 0.32\kappa \left(\frac{-\alpha g}{\kappa\nu}\right)^{1/3} (\Delta T_i)^{4/3} \left(\frac{\alpha \Delta T_i}{\beta \Delta S_i}\right)^2 \\ \psi_i &= \begin{cases} \frac{-\alpha}{\beta}\phi_i \left(1.85 + 0.85\left(\frac{\beta\Delta S_i}{\alpha \Delta T_i}\right)\right) & , 1 < \frac{\beta\Delta S}{-\alpha\Delta T} \leq 2 \\ -0.15\phi_i \left(\frac{\alpha}{\beta}\right) & , 2 < \frac{\beta\Delta S}{-\alpha\Delta T}. \end{cases} \end{aligned} \tag{8}$$

(Equations (8) appear slightly differently in [5] because we have followed the formalism of [15] and [4] and defined α as a negative value).

3.2.1 Evolution of initial layer

The equations describing the evolution of the initial layer are given by equation 4. When only one layer is present in the simulation, the magnitude of the interfaces are given by

$$\Delta T_1 = T_1 - \overline{T_t} \qquad \Delta S_1 = S_1 - \overline{S_t}. \tag{9}$$

$\overline{T_t}$ and $\overline{S_t}$ are the background temperature and salinity at the top of the staircase, which can be expressed as

$$\overline{T_t} = \overline{T}, \qquad \overline{S_t} = \overline{S_z} h_1 + \overline{S_0}, \tag{10}$$

where $\overline{S_0}$ is the initial salinity at the bottom of the system (Figure 8).

3.2.2 Evolution of multiple layers

Once two or more layers are present in the staircase, flux conservation laws are used to describe the evolution of the layers. The general form of these equations are

$$\rho c \frac{\mathrm{d}}{\mathrm{d}t}[h_i(T_i - \overline{T_i}] = \rho c(\phi_{i-1} - \phi_i), \qquad \frac{\mathrm{d}}{\mathrm{d}t}[h_i(S_i - \overline{S_i})] = \psi_i - \psi i - 1,$$

where ϕ_i and ψ_i are the fluxes through the ith layer.

$$\overline{T_i} = \overline{T}, \qquad \overline{S_i} = \overline{S_z}(d_i - h_i/2) + \overline{S_0}$$

are the background temperature and salinity imposed by the initial conditions, where $d_i = \sum_{j=1}^{i} h_j$.

3.2.3 Evolution of interior layers

Because $\overline{T_i}$,$\overline{S_i}$, and h_i are constant for all interior layers ($i < N$), equation (11) becomes

$$\rho c h_1 \frac{\mathrm{d}T_1}{\mathrm{d}t} = H - \rho c \phi_1, \qquad h_1 \frac{\mathrm{d}S_1}{\mathrm{d}t} = -\psi_1 \tag{11}$$

for the first layer, and

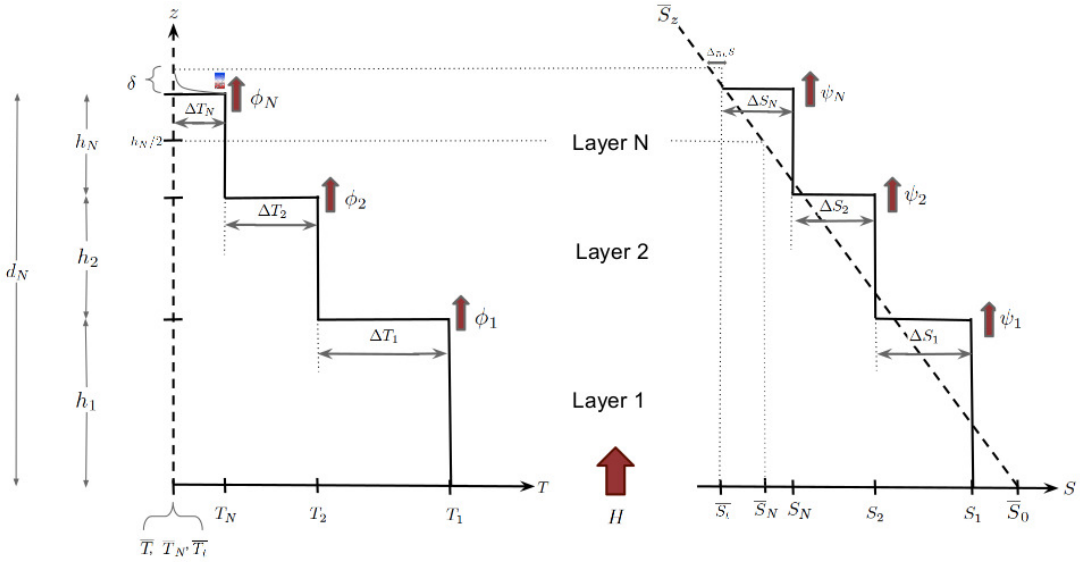

Figure 8: Cartoon depiction of the N-layer model.

$$h_r \frac{\mathrm{d}T_r}{\mathrm{d}t} = \phi_{r-1} - \phi_r, \qquad h_r \frac{\mathrm{d}S_r}{\mathrm{d}t} = \psi_{r-1} - \psi_r, \tag{12}$$

for all other layers, where $1 < r \leq N-1$.

3.2.4 Evolution of top layer

The thickness of the top layer grows with time, and the heat and salt flux exiting the top of the staircase are neglected, thus equation (11) becomes

$$\frac{\mathrm{d}}{\mathrm{d}t}\left(h_N(T_N - \overline{T_N})\right) = \phi_{N-1}, \qquad \frac{\mathrm{d}}{\mathrm{d}t}\left(h_N(S_N - \overline{S_N})\right) = \psi_{N-1}. \tag{13}$$

Finally, by satisfying equation (3), the third equation describing the top layer is

$$\alpha\left(T_N - \overline{T}_t\right) + \beta\left(S_N - \overline{S}_t\right) = 0.$$

Again, $\overline{T}_t = \overline{T}$, but now $\overline{S}_t = \overline{S}_z d_N + \overline{S}_0$.

3.2.5 Boundary layer

Equation (6) describes the evolution of the initial layer and boundary layer, with the adjusted boundary condition, $\theta(z = d_N) = T_N$. The criterion for overturn is given by equation (7) where, by assuming that the temperature profile of the boundary layer becomes relatively linear at the time of overturn, we let

$$\delta = \frac{2}{T_N - \overline{T_N}} \int_{d_N}^{\infty} \theta \mathrm{d}z.$$

3.2.6 Formation of new, N+1 layer

Once a boundary layer has overturned to form a new layer, the characteristics of this new layer are determined by conserving heat and salt and by satisfying equation (3):

$$\begin{aligned} \left(T_{N+1} - \overline{T}\right) h_{N+1} = \int_{d_N}^{\infty} \theta \mathrm{d}z, \qquad S_{N+1} &= \overline{S}_z \left(d_N + \frac{h_{N+1}}{2}\right) + \overline{S}_0 \\ \alpha \left(T_{N+1} - \overline{T}_t\right) + \beta \left(S_{N+1} - \overline{S}_t\right) &= 0, \end{aligned}$$

where the salinity at the top of the staircase has become $\overline{S}_t = \overline{S}_z \left(d_N + h_{N+1}\right) + \overline{S}_0$.

3.2.7 Merging layers

Lastly, if the density is neutral across an interface (i.e. $\alpha \Delta T + \beta \Delta S = 0$), the two layers will merge while conserving heat and salt. So the characteristics of the new layer are given by

$$\begin{aligned} T_{new} &= \frac{h_i T_i + h_{i+1} T_{i+1}}{h_i + h_{i+1}}, \qquad S_{new} = \frac{h_i S_i + h_{i+1} S_{i+1}}{h_i + h_{i+1}}, \\ h_{new} &= h_i + h_{i+1}. \end{aligned}$$

4 Adding thermobaric effects

The equations presented in the previous section differ slightly from those found in [4]. This is because they assume that $\overline{T} = \overline{S}_0 = 0$ and also because their equations are written using the following non-dimensional scaling where hatted variables indicate dimensional quantities:

$$t = \sqrt{S_*}\widehat{t}, \qquad z = \frac{S_*^{3/4}}{H_*^(1/2)} \widehat{z}, \qquad T = \frac{-\alpha_0 g \widehat{T}}{H_*^{1/2} S_*^{1/4}}$$
$$S = \frac{\beta g \widehat{S}}{H_*^{1/2} S_*^{1/4}}, \qquad \phi = \frac{-\alpha_0 g \widehat{\phi}}{H_*}, \qquad \psi = \frac{\beta g \widehat{\psi}}{H_*}.$$

The scaling for the buoyancy fluxes are defined as

$$H_* = \frac{-\alpha_0 g H}{\rho c}, \qquad S_* = \frac{-\beta g \overline{S_z}}{2}, \tag{14}$$

where α_0 is a constant, mean thermal expansion coefficient (note that this differs from $\widetilde{H}_*$).

In order to include thermobaric effects, we simply introduce a new, non-dimensional variable,

$$\alpha = \frac{\widehat{\alpha}}{\alpha_0}.$$

We set $\widehat{\alpha} = \alpha_0 + c\widehat{z}$, where c is determined by linearizing alpha near the local pressures of each experiment. The resulting equations using this non-dimensionalization are given below.

4.1 Heat and salt fluxes through interfaces

Non-dimensionalizing equations (8) leads to

$$\begin{aligned}
\phi &= 0.32\left(\frac{\alpha Q}{\sigma}\right)^{1/3}(\Delta T)^{4/3}\left(\frac{\alpha\Delta T}{\Delta S}\right)^{2} \\
\psi &= \begin{cases} \alpha\phi\left(1.85 - 0.85\left(\frac{\Delta S}{\alpha\Delta T}\right)\right), & 1 < \frac{\Delta S}{\alpha\Delta T} \le 2 \\ 0.15\alpha\phi, & 2 < \frac{\Delta S}{\alpha\Delta T}. \end{cases}
\end{aligned}$$

4.2 Growing 1st layer

Non-dimensionalizing equations (4) leads to

$$h_1 = \sqrt{\alpha t}, \qquad T_1 = \overline{T} + \sqrt{\frac{t}{\alpha}}, \qquad S_1 = \overline{S_0} - \sqrt{\alpha t}.$$

4.3 Evolution of interior layers

Non-dimensionalizing equations (11) and (12) leads to

$$\begin{aligned}
h_1\frac{\mathrm{d}T_1}{\mathrm{d}t} &= 1 - \phi_1, \qquad & h_1\frac{\mathrm{d}S_1}{\mathrm{d}t} &= \psi_1 \\
h_r\frac{\mathrm{d}T_r}{\mathrm{d}t} &= \phi_{r-1} - \phi_r, \qquad & h_r\frac{\mathrm{d}S_r}{\mathrm{d}t} &= \psi_{r-1} - \psi_r.
\end{aligned}$$

4.4 Evolution of top layer

Non-dimensionalizing equations (13) leads to

$$\begin{aligned}
\frac{\mathrm{d}}{\mathrm{d}t}\left(h_N(T_N - \overline{T_0})\right) &= \phi_{N-1}, \qquad & \frac{\mathrm{d}}{\mathrm{d}t}\left(h_N\right)) &= \psi_{N-1} - \frac{\mathrm{d}h_N}{\mathrm{d}t}(2d_N - \overline{S_0}) \\
\alpha(T_N - \bar{T}) &= S_N + 2d_N - \bar{S}_0.
\end{aligned}$$

After much algebra, these equations can be rewritten as

$$\begin{aligned}
\frac{\mathrm{d}h_N}{\mathrm{d}t} &= \frac{1}{2h_N}(\alpha\phi - \psi), \qquad \frac{\mathrm{d}T_N}{\mathrm{d}t} = \frac{1}{h_N}\left(\phi - \frac{T_N - \overline{T}}{2h}(\alpha\phi - \psi)\right) \\
\frac{\mathrm{d}S_N}{\mathrm{d}t} &= \frac{1}{h_N}\left(\psi - \frac{\alpha\phi - \psi}{2h_N}(S_N + 2d_N - \overline{S_0})\right).
\end{aligned}$$

4.5 Evolution of boundary layer

Non-dimensionalizing equations (6) and (7) leads to

$$\frac{\partial\theta}{\partial t} = Q\frac{\partial^2\theta}{\partial z^2}, \qquad R = \frac{\delta^3}{\sigma Q^2}\left(\alpha(T_N - \overline{T}) - \frac{2\sigma\delta}{\sigma+1}\right).$$

This is semi-analytically solved using the solution for heat through a finite, one-dimensional system with temperatures fixed on each boundary, where the length of the system, x_f, is chosen such that it is effectively infinity. Following [8], that semi-analytical solution is given by

$$\theta(x,t) = v + w, \qquad v(x) = T_N + (\overline{T} - T_N)\frac{x}{x_f} \tag{15}$$

$$w(x,t) = \sum_{n=1}^{N_{max}} b_n \sin\lambda_n x \exp -\lambda_n^2 kt, \qquad \lambda_n = \frac{n\pi}{x_f} \tag{16}$$

$$b_n = \frac{2}{x_f}\int_0^{x_f} -v(x)\sin\frac{n\pi x}{x_f}\mathrm{d}x. \tag{17}$$

4.6 Formation of new layer

Non-dimensionalizing equations (14) leads to

$$\begin{aligned}
\left(T_{N+1} - \overline{T}\right)h_{N+1} = \int_{d_N}^{\infty}\theta\mathrm{d}z \equiv \gamma, \qquad S_{N+1} &= -2\left(d_N + \frac{h_{N+1}}{2}\right) + \overline{S}_0 \\
\alpha\left(T_{N+1} - \overline{T}_t\right) + \left(S_{N+1} + 2(d_N + h_{N_1}) - \overline{S_0}\right) &= 0.
\end{aligned}$$

After much algebra, we find that this leads to

$$\begin{aligned}
h_{N+1} &= \sqrt{\alpha\gamma}, \qquad T_{N+1} = \overline{T} + \sqrt{\gamma/\alpha} \\
S_{N+1} &= \overline{S_0} - 2d_N - \sqrt{\gamma\alpha}.
\end{aligned}$$

4.7 Merge layers

Finally, while the criterion for merging becomes $\alpha\Delta T = \Delta S$, the equations which describe the new layer that results from merging (equations (14)), remain unchanged.

5 Preliminary results

To begin exploring how the thermobaric instability and double-diffusive convection interact, we first address the question of how the structure of the staircases may change as a function of α. One could imagine two possible outcomes of such an experiment. First, increasing α may have the same effect as increasing the heating rate or increasing the background temperature gradient. This would cause the density ratio to decrease as α increases, leading to a less stable system that transports heat and salt more efficiently. Alternatively, one could imagine that the steps might reorganize in such a way as to maintain its density ratio. In this case, the salinity interface would increase or the temperature interface would decrease, causing $\overline{S_z}/\overline{T_z}$ to increase and the density ratio to remain constant. Finally, in either case, we would expect the overall thickness of the layers to increase with α in order to sustain the larger interfaces or fluxes that would result in either scenario.

To try to answer this question, we ran our model using the same parameters that were used by [4] for a variety of αs. Specifically, we chose αs such that they were equivalent to systems where double-diffusive staircases are found in the deep and shallow Arctic, a laboratory and finally, one that would correspond to the Marianas trench, as a way to gauge how the staircases would behave for very large, yet realistic expansion coefficients (see Tables 1 and 2 for full description of parameters used). Although α is computed as a function of depth within each experiment, the staircases presented are sufficiently small that we may consider α to be constant.

Our results are presented in Figures 9-14. Figure 9 shows how the top of each layer evolves in time for each experiment and demonstrates that layers appear to form and merge more rapidly for larger values of α. This can be rationalized upon inspection of equation (7), the expression for R, which must reach a critical value in order for a new layer to form. One can see that R increases as a function of α and thus a smaller temperature gradient is required for overturn.

The rapid formation of layers also appears to correspond to rapid merging events. This might be because a layer that takes a short time to form will be smaller, less resilient and will then quickly have a similar density to the layer below compared to a layer that takes longer to form.

Secondly, the fourth subplot of Figures 12-14, which show the evolution of the layer heights for the first three layers and compares them to each experiment, demonstrate that once a quasi-steady layer forms (i.e. persists without merging immediately), it is likely to be larger when formed under conditions with a larger α. This result is consistent with what is observed in the shallow Arctic compared to the deep Arctic (see Figure staircase).

This result is further supported by Figures 10 and 11, which show the final form of the staircase at the end of each experiment. Moreover, one can see that the interfaces in salinity seem to increase as a function of α, while the temperature interfaces behave in the opposite manner. This can be explored further through the first and second subplots of Figures 12-14, which show how the two interfaces evolve for the first three layers. Although the result is far from indisputable, the same trend seems to exist, particularly for the more stable bottom two layers.

The size of the temperature interfaces, ΔT, are closely related to the fluxes across the interfaces (equation (8) but are also functions of α. These two quantities appear to have

opposite effects on both fluxes. Interestingly, the fifth and sixth subplots of Figures 12-14 clearly demonstrate that the heat flux decreases with α while the salt flux (even more strongly) increases with α. This implies that for the heat flux, the impact of ΔT outweighed that of α while the opposite was true for the salt flux. Again, these results are most clear for the more stable bottom two layers.

Lastly, we test our hypothesis from the beginning of this section and analyze how the density ratio varies for large changes in α. Upon inspection of the third and sixth subplot of Figures 12-14, it appears that the ratio of the two interfaces, $\Delta S/\Delta T$, increases with α, leaving the density ratio fairly constant by comparison (although there may be a small decrease as a function of α). This result suggests that increasing α has consequences which may not include destabilizing the water column but are reflected in the structure of the staircase.

Table 1: Simulation Parameters

κ	σ	H_*	S_*	T_{BG} (°C)	S_{BG} (psu)
$1.4 \cdot 10^{-7}$	7	$-1.48\alpha_0 \cdot 10^{-2}$	.167	.1	35

Table 2: Experiments

Description	α_0 (10^{-4} °C^{-1})	c (10^{-8} °C^{-1}m^{-1})	depth range (m)
lab	-.53	-2.88	0-.85
shallow Arctic	-.61	-2.86	292-316
deep Arctic	-1.24	-2.6	2611-2814
Marianas Trench	-2.92	-1.67	10800-10860

6 Implications, speculations and future work

Although we have not yet directly tested the effects of thermobaricity on double-diffusive staircases, these results help us to understand how the staircases change as a function of α. From our results, we might expect that in a system where thermobaric effects are important (i.e. α increases quickly with depth), the staircase will have certain features. First, we would expect that the layer thickness and salinity interfaces would increase with depth while the the temperature interfaces would decrease with depth (or increase less with depth , as this seems to be a necessary characteristic of all staircases). This in turn would lead to a divergent heat flux and a convergent salinity flux.

These results may explain why and how double-diffusive steps appear to increase with depth in nature. Furthermore, one could speculate that these thermobaric effects on the staircases may be important for understanding thermobaric convection. For example, between thermobaric overturning events, one might suspect that the system could be double-diffusively unstable (see Figure 3) and would therefore contain double-diffusive staircases. If the staircase supports converging and diverging vertical fluxes, they may impact the rate

at which the system reaches the density ratio required for the system to be thermobarically unstable.

However, these are merely speculations and require further scrutiny. Specifically, in the future we aim to determine how and under what conditions we might expect thermobaric effects to be important. This will be done by comparing experiments in which α is held constant to those in which α is allowed to vary appreciably within a staircase, based on the temperature gradient. We will explore a parameter range in which we will vary the heating rate, the salinity gradient and α. These experiments will include simulations with parameters that correspond to those found in the Antarctic as well as the shallow and deep Arctic, where both double-diffusion and thermobaricity may be important. This will hopefully lead us to a nice set of predictions that will allow us to begin to compare our results to observations.

7 Acknowledgements

A big thank you to the staff of the 2014 GFD summer school, particularly the organizers Glenn Flierl, Raffaele Farrari and Antonello Provenzale. The principal lecturers, Geoff Vallis and Kerry Emanuel are also acknowledged for impressively packing the cottage and packing our heads with knowledge. George Veronis is thanked for patiently waiting for our softball skills to arrive all summer. The friendship of the fellows and all of those who spent their summer on the porch helped make this summer especially fun. Finally, Mary-Louise Timmermans, George Veronis and Andy Ingersoll are warmly thanked for their time and supervision of this project.

References

[1] J. F. Adkins, A. P. Ingersoll, and C. Pasquero, *Rapid climate change and conditional instability of the glacial deep ocean from the thermobaric effect and geothermal heating*, Quaternary Science Reviews, 24 (2005), pp. 581–594.

[2] K. Akitomo, T. Awaji, and N. Imasato, *Open-ocean deep convection in the Weddell Sea: two-dimensional numerical experiments with a nonhydrostatic model*, Deep Sea Research Part I: Oceanographic Research Papers, 42 (1995), pp. 53–73.

[3] A. Gill, *Circulation and bottom water production in the Weddell Sea*, Deep Sea Research and Oceanographic Abstracts, 20 (1973), pp. 111–140.

[4] H. E. Huppert and P. F. Linden, *On heating a stable salinity gradient from below*, Journal of Fluid Mechanics, 95 (1979), p. 431.

[5] H. E. Huppert and J. S. Turner, *Double-diffusive convection and its implications for the temperature and salinity structure of the ocean and Lake Vanda*, Journal of Physical Oceanography, 2 (1972), pp. 456–461.

[6] T. B. Lø yning and J. E. Weber, *Thermobaric effect on buoyancy-driven convection in cold seawater*, Journal of Geophysical Research, 102 (1997), p. 27875.

[7] M. G. McPhee, *Marginal Thermobaric Stability in the ice-covered upper ocean over Maud Rise*, Journal of Physical Oceanography, 30 (2000), pp. 2710–2722.

[8] D. Powers, *Boundary Value Problems, Sixth Edition: and Partial Differential Equations*, Elsevier, 2006.

[9] T. Radko, *Double-Diffusive Convection*, Cambridge University Press, Cambridge, 2013.

[10] B. Rudels, E. P. Jones, U. Schauer, and P. Eriksson, *Atlantic sources of the Arctic Ocean surface and halocline waters*, Polar Research, 23 (2004), pp. 181–208.

[11] W. J. Shaw and T. P. Stanton, *Dynamic and double-diffusive instabilities in a weak pycnocline. Part I: Observations of heat flux and diffusivity in the vicinity of Maud Rise, Weddell Sea*, Journal of Physical Oceanography, 44 (2014), pp. 1973–1991.

[12] M.-L. Timmermans, L. Rainville, L. Thomas, and a. Proshutinsky, *Moored observations of bottom-intensified motions in the deep Canada Basin, Arctic Ocean*, Journal of Marine Research, 68 (2010), pp. 625–641.

[13] M.-L. Timmermans, J. Toole, R. Krishfield, and P. Winsor, *Ice-Tethered Profiler observations of the double-diffusive staircase in the Canada Basin thermocline*, Journal of Geophysical Research, 113 (2008), p. C00A02.

[14] J. Turner and H. Stommel, *A new case of convection in the presence of combined vertical salinity and temperature gradients*, Proceedings of the National Academy of Sciences, 52 (1964), p. 49.

[15] J. S. Turner, *The behaviour of a stable salinity gradient heated from below*, Journal of Fluid Mechanics, 33 (1968), pp. 183–200.

[16] G. Veronis, *On finite amplitude instability in thermohaline convection*, Journal of Marine Research, (1965), p. 1.

[17] G. WALIN, *Note on the stability of water stratified by both salt and heat*, Tellus, 16 (1964), pp. 389–393.

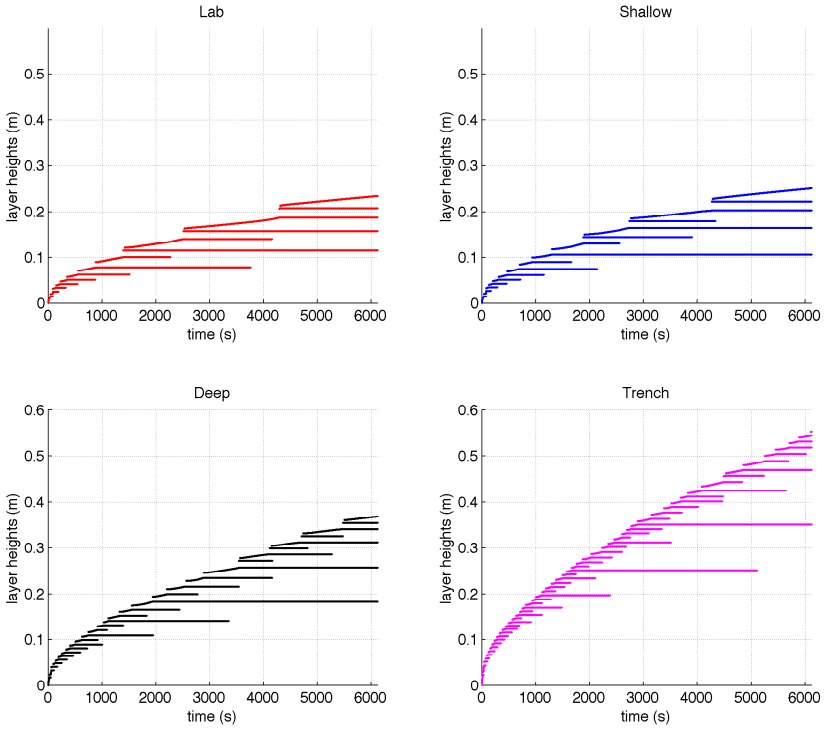

Figure 9: The evolution of the layer heights for the four experiments.

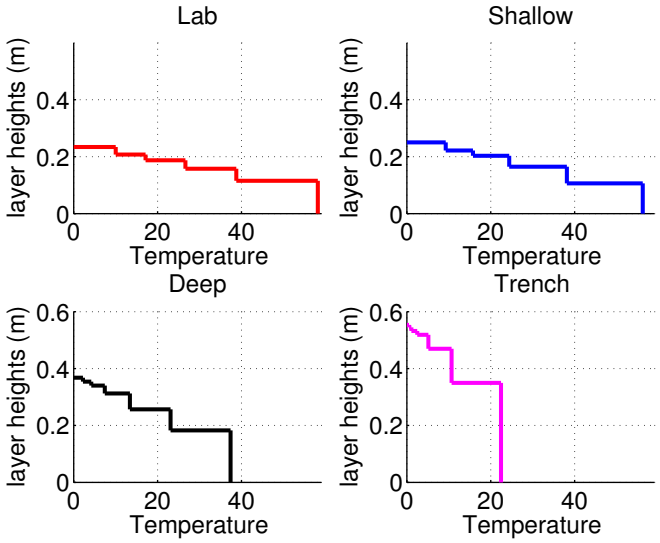

Figure 10: Final form of the staircases in temperature-depth space for the four experiments.

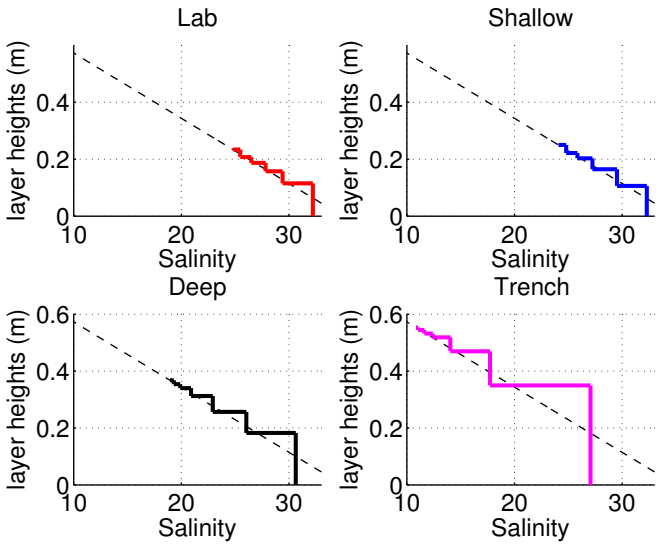

Figure 11: Final form of the staircases in salinity-depth space for the four experiments.

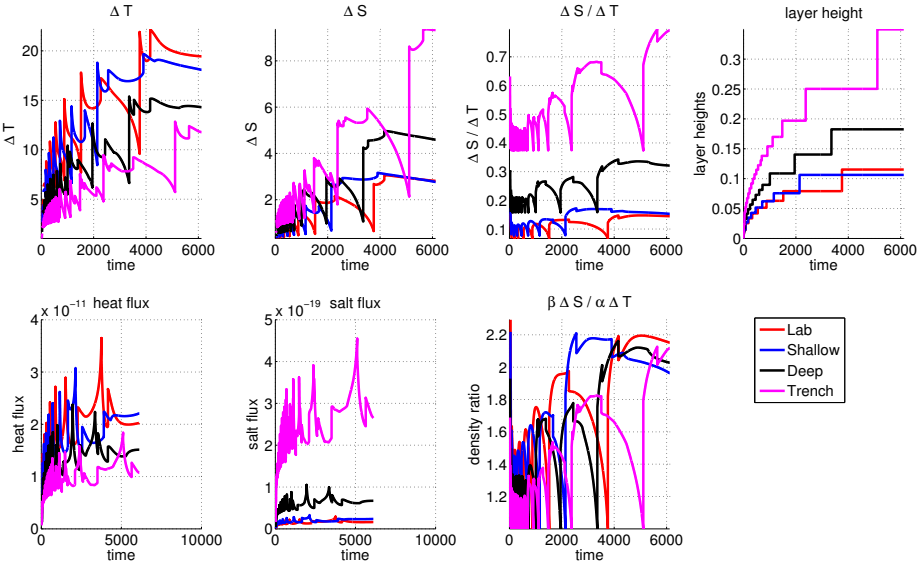

Figure 12: Comparison of the bottom layer between the four experiments. Evolution of the layer heights, magnitude and ratio of the interfaces, heat and salt fluxes, and density ratio is plotted.

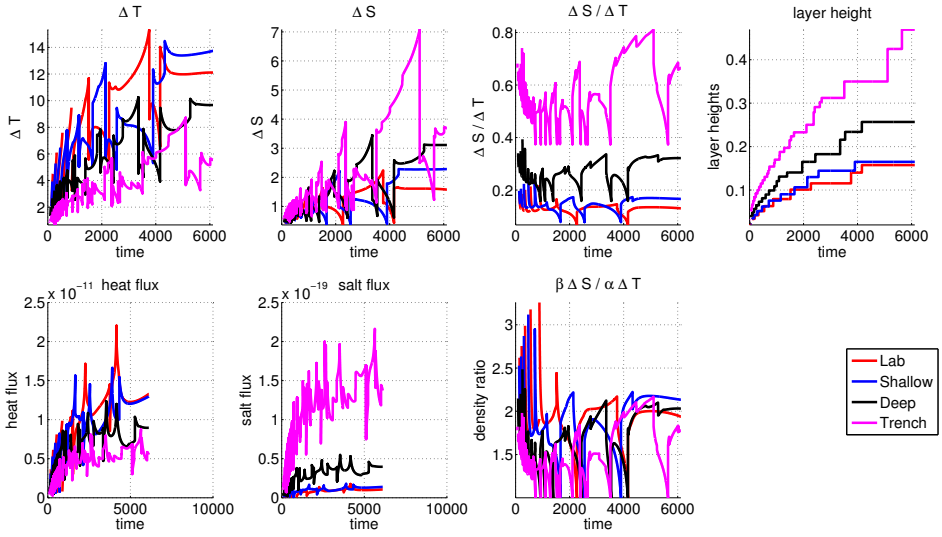

Figure 13: Comparison of the 2nd layer between the four experiments. Evolution of the layer heights, magnitude and ratio of the interfaces, heat and salt fluxes, and density ratio is plotted.

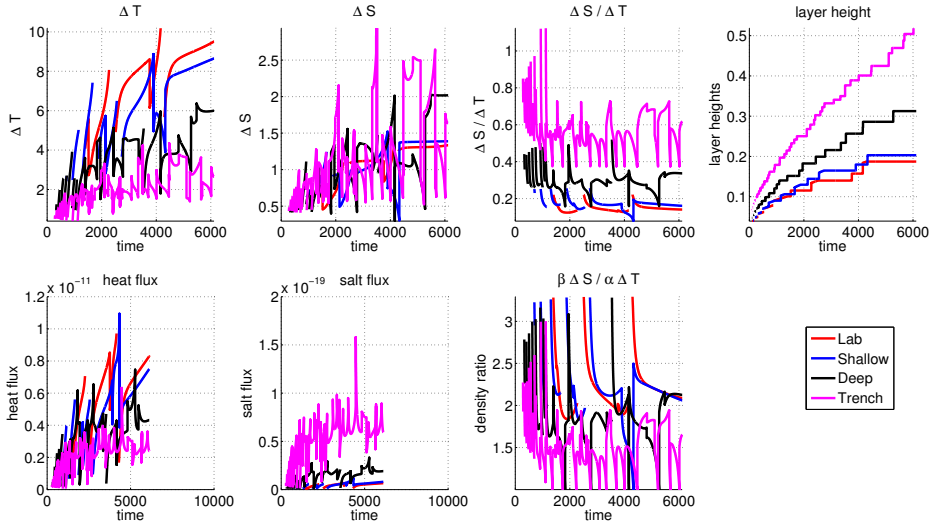

Figure 14: Comparison of the third layer between the four experiments. Evolution of the layer heights, magnitude and ratio of the interfaces, heat and salt fluxes, and density ratio is plotted.